DESIGN CONSIDERATIONS AND PERFORMANCE EVALUATION OF A 3-kW, SOFT-SWITCHED BOOST CONVERTER WITH ACTIVE SNUBBER

Yungtaek Jang and Milan M. Jovanović
DELTA Products Corporation
Power Electronics Laboratory
P.O. Box 12173, 5101 Davis Drive
Research Triangle Park, NC 27709, USA

Chau-Chun Wen
DELTA Electronics Inc.
3, Tung Yuan Road,
Chungli, Taiwan, R.O.C.

Abstract **-** The paper provides a complete design procedure of a high-power-factor (HPF) boost converter which employs an active snubber to reduce reverse-recovery related losses of the boost rectifier and achieve zero-voltage switching (ZVS) of the boost switch. The losses are reduced by inserting an inductor in the series path of the boost rectifier to reduce the di/dt rate during its turn-off. Extensive experimental evaluations of the performance of a 3-kW prototype for telecommunication applications operating from a 220 V_{rms} ± 20% input are presented. The evaluation results demonstrate that the HPF boost converter can operate at 100 kHz switching frequency with an efficiency in the 94-97% range at full power.

1. Introduction

A continuous-conduction-mode (CCM) boost converter is the preferred topology for implementing the front-end converter with active input-current shaping to the most telecommunication power supplies. However, since the dc-output voltage of the boost converter must be higher than the peak input voltage, the output voltage of the boost input-current shaper is relatively high. Due to the high output voltage, the converter requires the use of a high-voltage, fast-recovery boost rectifier. At high switching frequencies, fast-recovery rectifiers produce significant reverse-recovery-related losses when switched under "hard" switching conditions [1]. These losses can be significantly reduced and, therefore, a high efficiency can be maintained even at high switching frequencies by employing a soft-switching technique [2]-[8].

Recently, a new soft-switched boost converter and its variations have been proposed in [7]. The proposed scheme employs an auxiliary active switch with a snubber inductor and a capacitor to form an active snubber that is used to control the di/dt rate of the boost rectifier current and to create conditions for zero-voltage switching (ZVS) of the boost switch and the auxiliary active switch. This technique reduces the reverse-recovery-related losses by controlling the di/dt rate of the rectifier current with a snubber inductor which is connected in series with the path of the boost switch and rectifier. In addition, the energy stored in this inductor is used to discharge the output capacitance of the boost switch to zero prior to the switch turn-on, thus its capacitive turn-on switching loss is eliminated. The series connection of the auxiliary switch and the clamp capacitor, which is used to provide the discharging path of the snubber inductor current when the main switch is turned off, is connected to the output capacitor.

In this paper, a complete design procedure of this soft-switched boost converter for telecommunication applications and extensive experimental evaluations of its performance are presented. The evaluation was performed on a 3-kW prototype operating from a 220 V_{rms} ± 20%, single-phase input voltage. The evaluation results show that the input current shaping using the soft-switched boost converter can be performed with less than 5% THD at full output power and the nominal input voltage. In addition, experimental results demonstrate that current harmonics of the input current satisfy the IEC1000-3-2 standard over the entire input voltage and output power ranges. The experimental HPF boost converter operates with an efficiency range of 94-97% at full power and 100 kHz switching frequency.

2. Review of Soft-Switched Boost Converter with Active Snubber [7]

The circuit diagram of the boost converter which employs the active snubber for reverse-recovery-loss reduction is

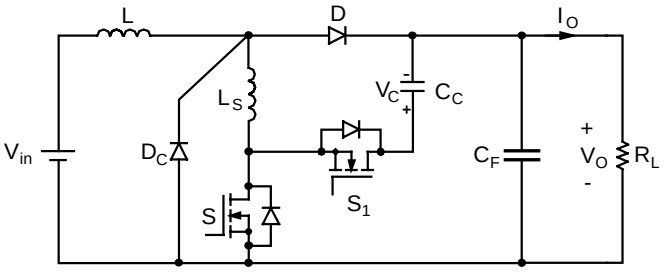

Fig. 1 Boost power stage with active snubber.

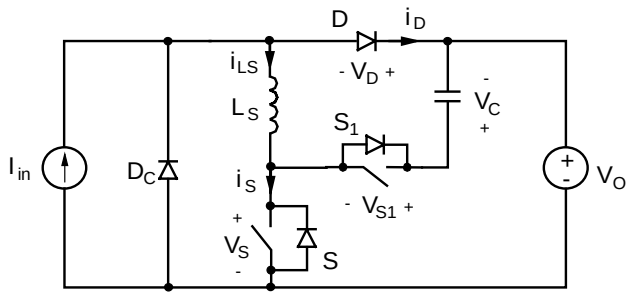

Fig. 2 Simplified circuit diagram of the proposed boost power stage showing reference directions of currents and voltages.

shown in Fig. 1. The circuit in Fig. 1 uses a snubber inductor L_S, which is connected in series with the boost switch S and rectifier D, to control the di/dt rate of the rectifier when boost switch S is turned on. In addition, the series connection of auxiliary switch S_1, clamp capacitor C_C is used to discharge the energy stored in the inductor to the output after S_1 is turned off. Diode D_C is employed to eliminate the parasitic ringing between the junction capacitance of rectifier D and the snubber inductor by clamping the anode of D to ground.

Figs. 2 and 3 show the circuit diagram of the simplified converter and the topological stages of the circuit during a switching cycle, respectively. To simplify the analysis of operation, it is assumed that the inductance of boost inductor L is large so that it can be represented by constant-current source I_{in}, and that the output-ripple voltage is negligible so that the voltage across the output filter capacitor can be represented by constant-voltage source V_O.

The boost and auxiliary switches in Fig. 3 never conduct simultaneously. In fact, the proper operation of the power stage, *i.e.*, the operation which reduces reverse-recovery related losses and enables soft switching, requires appropriate dead times between the turn-off of boost switch S and turn-on of auxiliary switch S_1, and vice versa. Before main switch S is turned off at $t = T_0$, the entire input current, I_{in}, flows through inductor L_S and switch S. At the same time, rectifier D is off with a reverse voltage across its terminals equal to output voltage V_O. Auxiliary switch S_1 is also off, blocking the voltage $V_O + V_C$, where V_C is the voltage across clamp capacitor C_C.

After switch S is turned off at $t = T_0$, the current which was flowing through the channel of the MOSFET of switch S is diverted to the output capacitance of the switch, C_{OSS}, as shown in Fig. 3(a). As a result, the voltage across switch S starts to increase linearly due to the constant charging current I_{in}. At the same time, voltage V_{S1} across switch S_1 decreases at the same rate. Because inductor current i_{LS} continues to charge C_{OSS} after v_S reaches V_O, V_S continues to increase above V_O, causing the current through inductor L_S to start decreasing due to a negative voltage across its terminals. This topological stage ends at $t = T_1$, when voltage V_{S1} reaches

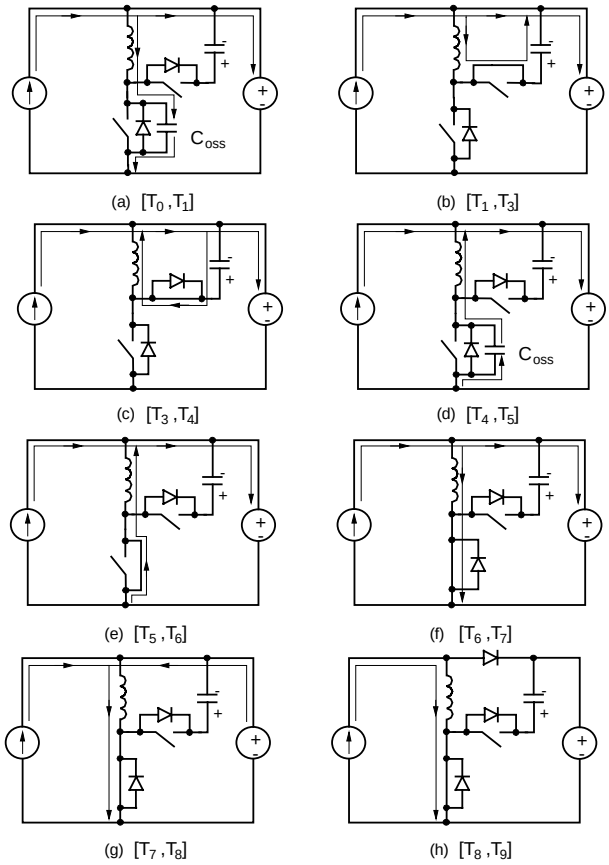

Fig. 3 Topological stages of the proposed boost power stage.

zero, *i.e.*, when the anti-parallel diode of switch S_1 starts conducting. At that moment, the remaining inductor current i_{LS} is diverted into clamp capacitor C_C, as shown in Fig. 3(b).

During the topological stage shown in Fig. 3(b), inductor current i_{LS} continues to decrease as the energy stored in L_S continues to be transferred into clamp capacitor C_C. This topological stage ends at $t = T_3$, when i_{LS} reaches zero, and the anti-parallel diode of auxiliary switch S_1 stops conducting. To achieve ZVS of S_1, it is necessary to turn on the transistor of switch S_1 while its anti-parallel diode is conducting. If the transistor of switch S_1 is turned on prior to $t = T_3$, inductor current i_{LS} will continue to flow after $t = T_3$ in the opposite direction through the closed transistor of switch S_1, as shown in Fig. 3(c). During this topological stage, the energy stored in clamp capacitor C_C during interval $[T_1 - T_3]$ is returned to the inductor in the opposite direction. This interval ends at $t = T_4$ when auxiliary switch S_1 is turned off.

When, at $t = T_4$, S_1 is turned off, i_{LS} is forced to flow through output capacitance C_{OSS} of boost switch S, as shown in Fig. 3(d). Since in this topological stage i_{LS} discharges C_{OSS}, boost-switch voltage V_S decreases towards zero. As a result, the anti-parallel diode of S will start conducting as shown in Fig. 3(e). To achieve ZVS of switch S, it is

necessary to turn on the transistor of switch S during the time interval [T_5 - T_6], when the anti-parallel diode of S is conducting. If the transistor of S is turned on during this interval, i_{LS} will continue to increase linearly after $t = T_6$, as shown in Fig. 3(f). At the same time, rectifier current i_D will continue to decrease linearly. The rate of the i_D decrease is determined by the value of L_S inductance because

$$\frac{di_D}{dt} = -\frac{V_O}{L_S}. \quad (1)$$

To reduce the rectifier-recovered charge and the associated losses, a proper L_S inductance needs to be selected. Generally, a larger inductance, which gives a lower di_D/dt rate, results in a more efficient reduction of the reverse-recovery-associated losses [1].

The linear increase of i_{LS} should stop at $t = T_7$, when i_{LS} reaches the input-current level I_{in}, and rectifier current i_D falls to zero. However, due to the residual stored charge, rectifier current i_D starts flowing in the reverse direction, as shown in Fig. 3(g), producing an overshoot of the switch current over the I_{in} level. Without L_S, this reverse-recovery current would be many times larger. Once the rectifier has recovered at $t = T_8$, the entire input current I_{in} flows through switch S (Fig. 3(h)), until the next switching cycle is initiated at $t = T_9$.

Besides the stored charge that needs to be recovered before fast-recovery rectifier D can block voltage, the rectifier possesses a junction capacitance. In a practical boost circuit, this capacitance interacts with the snubber inductance causing an undesirable parasitic ringing of the rectifier voltage after the rectifier has recovered. As explained in [7] and [8], the ringing can be completely eliminated by the addition of diode D_C, shown in Fig. 1.

3. Design of a 3-kW, HPF Boost Rectifier

3.1 Specifications

The 3-kW, HPF boost experimental rectifier was designed for the following specifications.

Input

- Voltage V_{in}: 1-phase, 220 $V_{(L\text{-}L,rms)}$ ± 20%
- Line Frequency f_L: 47 - 63 Hz
- THD: < 5%
- Power Factor: > 0.99 (100% load)

Output

- Voltage V_0 : 400 V_{dc} ± 2% (0 - 100% load)
- Power P_0 : 3 kW
- Ripple Voltage: < 6.5 $V_{peak\text{-}peak}$ (300/360 Hz)
- Switch Frequency f_S : 100 kHz

Cooling

- Force Convection

3.2 Design of Active Snubber Circuit

Figure 4 shows typical stored charge of a fast-recovery rectifier vs. the rate of rectifier-current change di_D/dt. To reduce the reverse-recovery-related losses, the di_D/dt rate of the majority of fast-recovery rectifiers should be kept below approximately 100 A/μs [1]. Generally, slower rectifiers require slower di_D/dt rates than faster rectifiers to achieve the same level of reduction of the reverse-recovery-related losses. As a rule of thumb, the practical range of snubber inductance L_S is from to 2 μH to 20 μH. As can be seen from Fig. 4, stored charge Q_{rr} of a fast-recovery rectifier at 15 A and with di_D/dt = 1000 A/μs is approximately 500 nC which is four times greater than the stored charge with di_D/dt = 100 A/μs. In fact, without a snubber, the rate of rectifier-current change is mainly decided by parasitic inductance L_P of the trace between boost switch S and rectifier D, which is generally less than several hundreds nano henry. As a result, the rate of rectifier-current change of the boost rectifier without a snubber inductor is approximately 2000 A/μs (V_O/L_P = $400/0.2\times10^{-6}$). To reduce the stored charge which is directly proportional to reverse-recovery-related losses, snubber inductor L_S must be added.

Generally, the maximum value of snubber inductance L_S is limited by the voltage stress on switch S and auxiliary switch

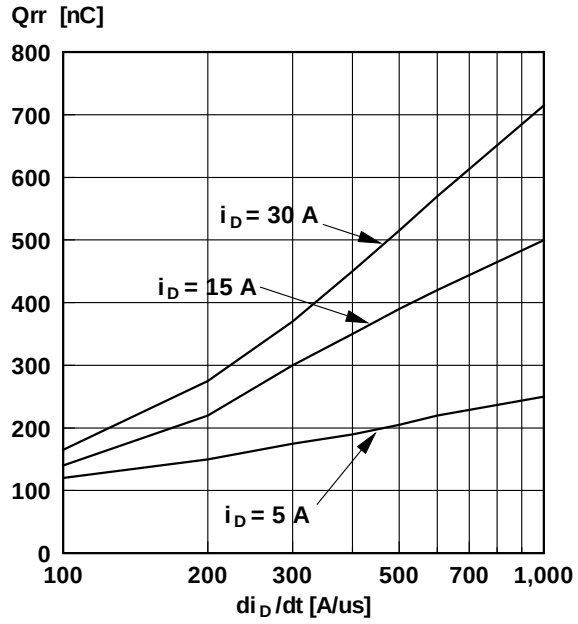

Fig. 4 Typical stored charge of a fast-recovery rectifier vs. di_D/dt at 125°C, where di_D/dt is the rate of rectifier-current change through zero crossing [1].

S_1. As can be seen from Fig. 2, the voltage stress of switches S and S_1 are the same and equal to $V_O + V_C$. During the period when boost switch S is on, auxiliary switch S_1 blocks the voltage which is the summation of the clamp capacitor voltage and the output voltage. Boost switch S blocks the same voltage when auxiliary switch S_1 is on. Compared to the corresponding stress in the conventional, "hard"-switched boost converter, the voltage stress of boost switch S in the proposed converter is higher for the amount of clamp voltage V_C. To keep the voltage stress of switches S and S_1 within reasonable limits, it is necessary to properly select clamp-voltage level V_C. Clamp-capacitor voltage V_C, can be expressed as

$$V_C = 2L_S f_S I_O \left| \frac{V_O}{V_{in}} \right|^2, \quad (2)$$

where f_S is the switching frequency. Detailed derivations and explanations can be found in [7].

According to Eq. (2), V_C is the maximum at full load $I_{o(max)}$ and low line $V_{in(min)}$, since switching frequency f_S and output voltage V_O are constant. For given input and output specifications, *i.e.*, for given $I_{o(max)}$, $V_{in(min)}$, f_S, and V_O, the voltage stresses on the main and auxiliary switches can be minimized by minimizing snubber inductor L_S. From the specifications, the minimum input voltage $V_{in(min)}$ = 176 V, the maximum output current $I_{O(max)}$ = 7.5 A, switching frequency f_S = 100 kHz, and output voltage V_O = 400 V. To limit the maximum voltage stress of switches below 85% of the voltage rating of a 500-V switch, the maximum clamp-capacitor voltage $V_{C(max)}$ should be less than 40 V. As a result, the value of snubber inductor L_S was chosen to be approximately 5 μH. This value results in 80 A/μs di_D/dt rate.

Since the average voltage across the clamp-capacitor is independent from the size of the clamp capacitor C_C as shown in Eq. (2), the value of C_C can be designed to minimize the switch-frequency voltage ripple. The energy stored in the snubber inductor contributes to the voltage ripple during a switching cycle. The maximum switch-frequency voltage ripple $V_{C(P-P)}$ can be expressed as

$$V_{C(P-P)} = I_{O(max)} \sqrt{\frac{L_S}{C_C}}. \quad (3)$$

The choice of four 2.2 μF ceramic capacitors in parallel for the clamp capacitor limits the magnitude of the maximum peak-to-peak ripple voltage to approximately 5 V.

To achieve ZVS of main switch S, it is necessary that the energy stored in L_S at the moment auxiliary switch S_1 is turned off be larger than or equal to the energy required to discharge output capacitance C_{OSS} of switch S from $V_O + V_C$ down to zero, *i.e.*, if

$$\frac{1}{2} L_S I_{O(max)}^2 \geq \frac{1}{2} C_{OSS} \left(V_O + V_C \right)^2, \quad (4)$$

then the switch voltage will reach zero. Since the energy stored in L_S is proportional to the square of the output (load) current, it is easier to satisfy the ZVS condition at heavier loads than at lighter loads. As a result, at light loads switch S does not operate with ZVS. On the other hand, auxiliary switch S_1 operates with ZVS in virtually the entire load range, because it uses energy stored in boost inductor L, which is much larger than that stored in snubber inductor L_S, to discharge its output capacitance. For L_S = 5 μH, the boost switch operates with zero-voltage switching down to 30% of the full load at the minimum line.

In input-current-shaping applications, the circuit in Fig. 1 needs an additional rectifier to prevent the voltage across clamp capacitor C_C from becoming negative. Namely, due to the varying line voltage and constant output voltage, the duty cycle of the boost-converter input-current shaper varies. It is close to 100% around the zero crossings of the line voltage, and it is smallest at the peak of the line voltage. When the line voltage is around zero, the energy stored in the boost inductor is small even with the switch duty cycle close to 100%. As a result, after switch S is turned off, the inductor stored energy is not sufficient to charge output capacitance C_{OSS} of S up to $V_O + V_C$, and force the conduction of the anti-parallel diode of auxiliary switch S_1. Since around zero crossings of the line voltage anti-parallel diode of S_1 does not conduct, consequently, capacitor C_C does not charge to the positive direction. However, clamp capacitor C_C may be reversely charged for a brief duration of switch S_1 conduction near zero crossing. If V_C becomes negative, no reset voltage for the core of the snubber inductor will be available, and the core would saturate. To prevent V_C from becoming negative, clamp diode D_{C1} (typically the Schottky type) should be added to the active clamp as shown in Fig. 5.

3.3 Component

Semiconductors

The peak voltage stress on switch S is approximately 440 V as shown in Section 3.2. The peak current stress on S, which is equal to the peak input current is approximately 25.7 A at full load and low line. An IXFN 48N50 MOSFET from IXYS (V_{CES} = 500 V, I_{C25} = 48 A, R_{DS} = 0.1 Ω) was used for boost switch S. To use a common heatsink for boost switch S, active snubber switch S_1, and output diode D, devices of the similar package were selected. Since the peak voltage stress on snubber switch S_1 is equal to the boost switch, An IXFN 44N50 MOSFET from IXYS (V_{CES} = 500 V, I_{C25} = 44 A, R_{DS} = 0.12 Ω) was used for S_1.

Since, output diode D must block the output voltage of 400 V and must conduct a peak load current of 7.5 A, a DSEI 2x61-06 diode from IXYS (V_{RRM} = 600 V, I_{FAVM} = 60 A, t_{rr} = 35 ns) was used for output diode D. To reduce the conduction loss of the output diode, a device which has higher current rating than the designed maximum current was selected. The voltage stress of clamp diode D_C is the same as output voltage V_O. However, since the circulating current through L_S-D_C loop is small, the power dissipation of clamp diode D_C is negligible [7]. Threrfore, a RHRP860 diode from Harris (V_{RRM} = 600 V, I_{FAVM} = 8 A, t_{rr} = 30 ns) was used for D_C. For D_{C1} which carries only transient current during input-voltage zero crossing and prevents the reverse voltage of clamp capacitor C_C, a MBR10100 Schottky diode from Motorola (V_{RRM} = 100 V, I_{FAVM} = 10 A) was selected.

Boost inductor

Since the desired inductance of boost inductor L is 0.45 mH, boost inductor L was built using two toroidal cores attached in parallel (Magnetics, Kool-μ 77110-A7) and 55 turns of magnet wire (AWG #13). Two toroidal cores are used in parallel to reduce the flux density and number of turns of the winding.

Snubber inductor

The desired inductance of the snubber inductor is 5 μH to obtain the desired di/dt and limit the clamp capacitor voltage. Snubber inductor L_S was built using two toroidal cores attached in parallel (Magnetics, MPP 55550-A2) and 9 turns of magnet wire (AWG #13).

Capacitors

Four 2.2 μF, 100 VDC, ceramic capacitors in parallel are used for the clamp capacitor C_C to limit the magnitude of the maximum peak-to-peak ripple voltage to approximately 5 V. Since the peak clamping capacitor voltage is approximately 40V for this prototype, 100 VDC ceramic capacitors are utilized.

4. Experimental Results

The performance of the boost converter with the active snubber was evaluated on a 3 kW (400 V/ 7.5 A), line-voltage (176 - 264 V_{ac}) power-factor-correction circuit operating at 100 kHz. The component values of the experimental circuit are shown in Fig. 5.

The control circuit was implemented with the average-current PFC controller UC3854. The TC4420 driver is used to generate the required gate-drive signal for the main switch. The TSC429 driver with an isolation transformer are used to generate the required gate-drive signal for the auxiliary switch.

With the selection of L_S = 5 μH, the di/dt turn-off rate of the rectifier was limited to $di_D/dt = V_O/L_S$ = 80 A/μs. In addition, the maximum voltage of clamp capacitor C_C, which occurs at the minimum line voltage and full load, was limited to approximately 40 V. With $V_{C(max)}$ = 40 V, the maximum voltage stresses on the switches were limited to $V_O + V_{C(max)}$ = 440 V.

Figure 6 shows the gate-drives, main-switch drain-to-source, and boost rectifier voltage waveforms of the experimental converter operating at the minimum line (V_{in}^{min} = 176 V_{ac}) and full power of 3 kW. As can be seen from Fig. 6(a), the voltage stress on the main switch is approximately 430 V. Also, from Fig. 6(b), which shows an enlarged turn-on transition of the waveforms in Fig. 6(a), it can be seen that boost switch S turns on when the voltage across it is zero. As a result of the zero-voltage switching of S, its turn-on output-capacitance discharge loss is eliminated. For L_S = 5 μH, the experimental converter can operate with zero-voltage switching down to 30% of the full load at the minimum line voltage.

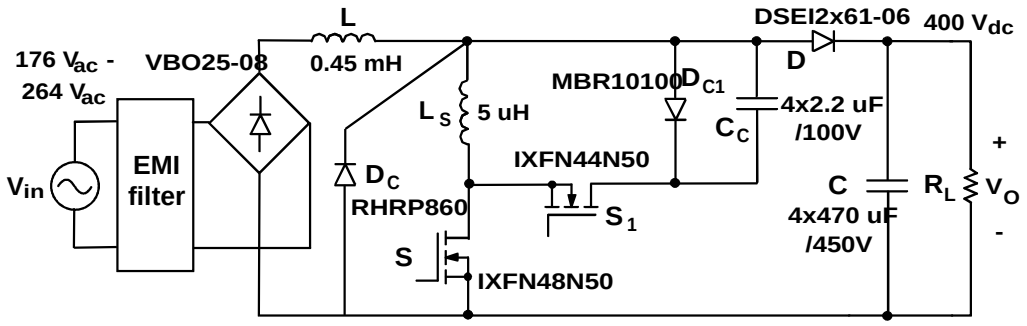

Fig. 5 Experimental 3 kW, boost power stage with active-clamp snubber.

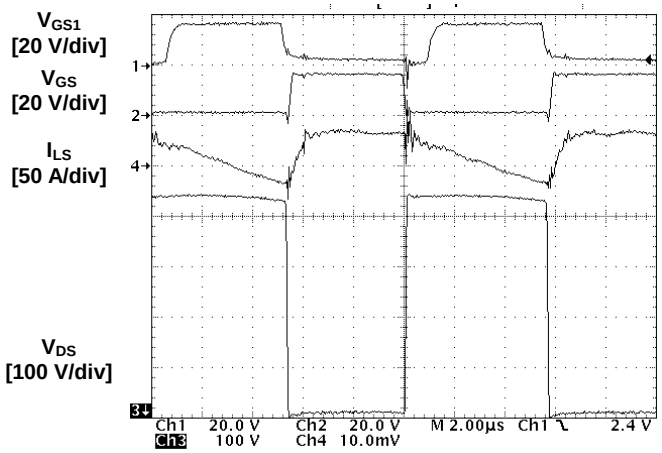

(a)

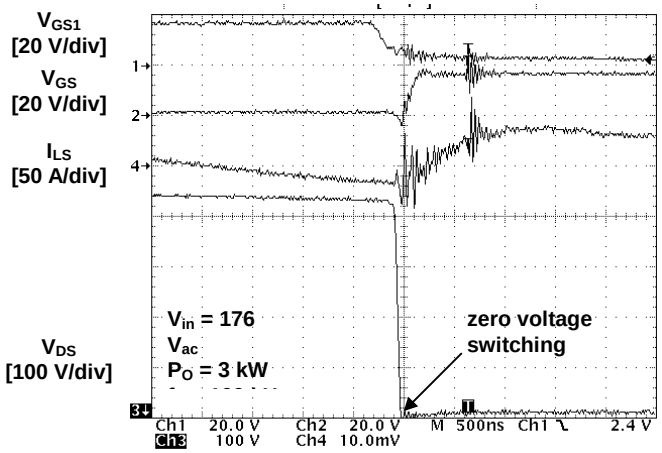

(b)

Fig. 6 Oscillograms of gate-drive voltages V_{GS} and V_{GS1}, snubber inductor current I_{LS}, and boost-switch drain-to-source voltage V_{DS} waveforms at low line (176 V_{ac}) and full power (3 kW): (a) 2 µs time base; (b) 500 ns time base.

Figure 7 shows the measured efficiencies of the experimental converter with (solid lines) and without (dashed lines) the active snubber at the minimum and maximum line voltages as functions of the output power. As can be seen from Fig. 7, for both line voltages the active snubber improves the conversion efficiency in the entire measured power range (1 kW to 3 kW). Nevertheless, the efficiency improvement is more pronounced at the minimum line and higher power levels where the reverse-recovery losses are greater. Specifically, at the maximum line (265 V_{ac}), the efficiency improvement at 3 kW is 0.7%. However, at the minimum line, the implementation without the active snubber cannot deliver more than approximately 2.4 kW due to the thermal runaway of the switch caused by excessive reverse-recovery losses. Even at P_O = 2.4 kW, the active snubber improves the efficiency by approximately 1%, which translates into approximately 20% reduction of the losses.

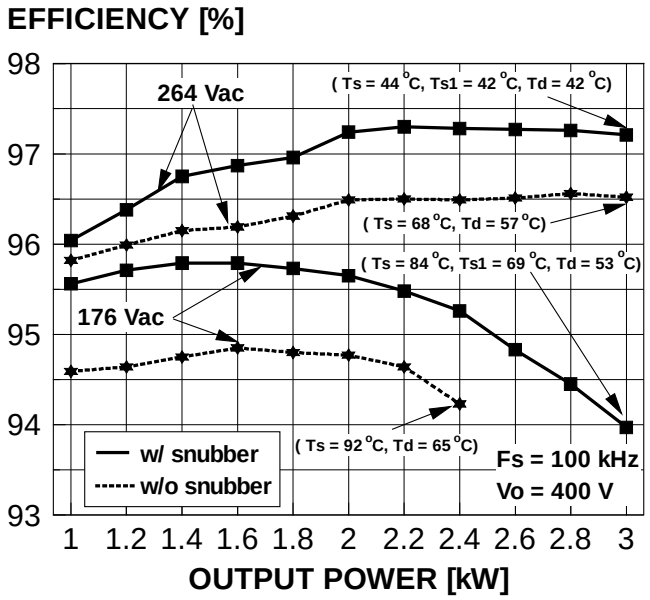

Fig. 7 Measured efficiencies of the experimental converter with (solid lines) and without (dashed lines) active snubber at the minimum and maximum line voltages as functions of the output power. Note that the maximum possible output power for the implementation without the snubber is limited to 2.4 kW.

Figure 8 shows the measured temperatures of the experimental converter with (solid lines) and without (dashed lines) the active snubber at the minimum line voltage as functions of the output power. The ambient temperature was approximately 29°C during the measurement. As can be seen from Fig. 8, at the same power levels, the temperatures of the semiconductor components in the implementation with the active snubber are significantly lower than those in the implementation without the snubber. As indicated in Figs. 7 and 8, at the maximum line (265 V_{ac}) and full power (3 kW), the case temperatures of the boost rectifier and boost switch in the implementation with the snubber are T_d = 42 °C and T_S = 44 °C, respectively, whereas the corresponding temperatures in the implementation without the snubber are T_d = 57 °C and T_S = 68 °C. Similarly, at the minimum line voltage (176 V_{ac}) and full power, the rectifier and switch temperatures in the implementation with the snubber are T_d = 53 °C and T_S = 84 °C. As can be seen from Figs. 7 and 8, the implementation without the snubber cannot deliver the full power of 3 kW at the minimum line because the rectifier becomes thermally unstable at approximately 2.4 kW. In fact, for the implementation without the snubber the temperature of the boost rectifier is T_S = 92 °C at 2.4 kW, which is

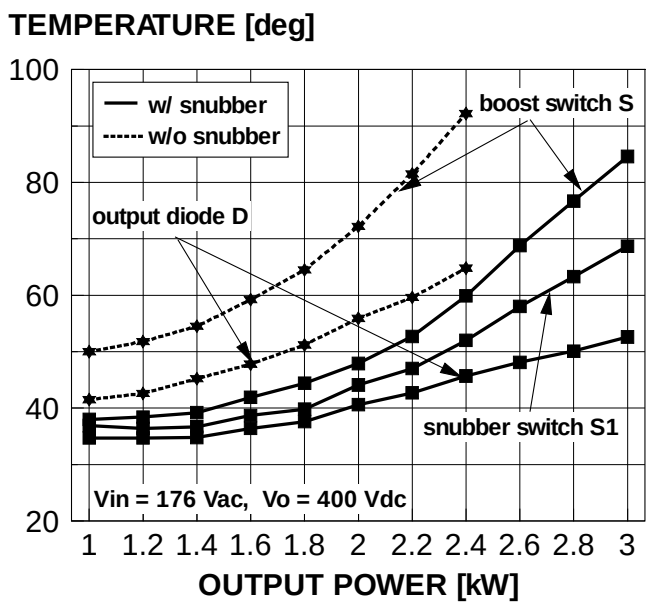

Fig. 8 Measured switch temperature of the experimental converter with (solid lines) and without (dashed lines) active snubber at the minimum line voltage as functions of the output power.

significantly higher than the temperature of the rectifier (T_d = 60 ^{O}C) in the implementation with the snubber at the same output power.

Figure 9 shows the measured waveform of the input line current of the prototype rectifier delivering 3 kW at 220 V input voltage. Since the maximum duty cycle is not limited by the addition of the active snubber circuit, the input current waveforms with and without the active snubber circuit are nearly identical.

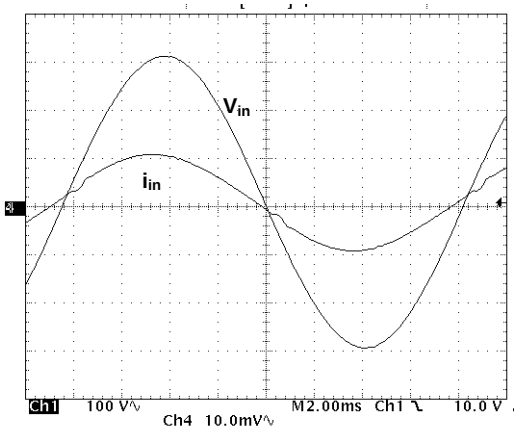

Fig. 9: Input voltage V_{in} (100 V/div) and input current i_{in} (20 A/div) waveforms at V_{in} = 220 V_{rms}, THD = 3.6%, PF = 99.3.

5. Conclusion

An active-snubber technique which reduces the reverse-recovery-related losses and reduces the capacitive-discharge turn-on switching loss of the boost converter has been described. Also, a complete design procedure of a HPF boost converter with the active snubber circuit and extensive experimental evaluations of its performance on a 3-kW prototype for telecommunication applications are presented. The evaluation results demonstrate that the HPF boost converter at 100 kHz switching frequency operates with an efficiency in the 94-97% range at full power.

The results of the experimental evaluation have shown that the proposed active-snubber technique can significantly extend the maximum power range at which a fast-recovery rectifier can be reliably applied.

References

[1] Y. Khersonsky, M. Robinson, D. Gutierrez, "New fast recovery diode technology cuts circuit losses, improves reliability," *Power Conversion & Intelligent Motion (PCIM) Magazine*, pp. 16 - 25, May 1992.

[2] R. Streit, D. Tollik, "High efficiency telecom rectifier using a novel soft-switched boost-based input current shaper," *International Telecommunication Energy Conf. (INTELEC) Proc.*, pp. 720 - 726, Oct. 1991.

[3] G. Hua, C.S. Leu, F.C. Lee, "Novel zero-voltage-transition PWM converters," *IEEE Power Electronics Specialists' Conf. (PESC) Rec.*, pp. 55 - 61, June 1992.

[4] D.C. Martins, F.J.M. de Seixas, J.A. Brilhante, I. Barbi, "A family of dc-to-dc PWM converters using a new ZVS commutation cell," *IEEE Power Electronics Specialists' Conf. (PESC) Rec.*, pp. 524 - 530, June 1993.

[5] J. Bassett, "New, zero voltage switching, high frequency boost converter topology for power factor correction," *International Telecommunication Energy Conf. (INTELEC) Proc.*, pp. 813 - 820, Oct. 1995.

[6] C.M.C. Duarte, I. Barbi, "A new family of ZVS-PWM active-clamping dc-to-dc boost converters: analysis, design, and experimentation," *International Telecommunication Energy Conf. (INTELEC) Proc.*, pp. 305 - 312, Oct. 1996.

[7] M.M. Jovanovi}, "A technique for reducing rectifier reverse-recovery-related losses in high-voltage, high-power boost converters," *IEEE Applied Power Electronics (APEC) Conf. Proc.*, pp. 1000 - 1007, Mar. 1997.

[8] C.M.C. Duarte, I. Barbi, "An improved family of ZVS-PWM active-clamping dc-to-dc converters," *IEEE Power Electronics Specialists' Conf. (PESC) Rec.*, pp. 669 - 675, June 1998.